Electrochimica Acta 489 (2024) 144256

Contents lists available at ScienceDirect

Electrochimica Acta

journal homepage: www.journals.elsevier.com/electrochimica-acta

Enhancing electrochemiluminescence intensity through emission layer control

Chiara Mariani [a], Sara Bogialli [b], Francesco Paolucci [a], Paolo Pastore [b], Alessandra Zanut [b,*], Giovanni Valenti [a,*]

[a] Department of Chemistry "Giacomo Ciamician", Alma Mater Studiorum University of Bologna, Via Selmi 2, Bologna 40126, Italy
[b] Department of Chemical Sciences, University of Padova, via Marzolo 1, Padova 35131, Italy

ARTICLE INFO

Keywords:
Electrochemiluminescence
Imaging
Beads based assay
Biosensor
Microscopy
Cell
Scanning electrochemical microscopy

ABSTRACT

Electrochemiluminescence (ECL), an intriguing luminescent phenomenon induced by electrochemical stimulation, has evolved from studying electron transfer reactions to a powerful analytical method and imaging technique. ECL can be generated through annihilation or co-reactant methods, with recent advancements integrating it into imaging devices for diverse applications. This review traces the evolution of ECL from its early applications to recent developments in imaging technology. Notably, the utilization of charge-coupled devices (CCD) and electron multiplying charge-coupled devices (EMCCD) in ECL microscopy has revolutionized imaging capabilities, making it a cost-effective option for point-of-care testing. The review explores the heterogeneous ECL mechanism, emphasizing its limitations and challenges in visualizing objects away from the electrode surface. The synergy between ECL and microscopy is highlighted, showcasing its diverse applications and contributions to understanding ECL mechanisms and improving its use in biological contexts. Finally, the review encapsulates innovative approaches in material design, surface modification, and electrode architecture, providing a comprehensive overview of strategies to control the active layer of the ECL and advance ECL microscopy.

1. Introduction

Electrochemiluminescence (ECL), also known as electrochemically generated chemiluminescence, is a luminescent occurrence triggered by electrochemical stimulation. ECL relies on the electrochemical generation of substances that engage in high-energy electron transfer reactions, leading to the formation of illuminated excited states [1].

ECL can essentially be produced through either the annihilation or the co-reactant method. In the annihilation process, the luminophores are electrochemically reduced and oxidized at the cathode and anode, respectively (or at a single electrode by pulsing the applied potential alternately) to produce radicals. These radicals then combine to form the excited species. The co-reactant approach, on the other hand, involves a solution reagent that is either reduced (via the reductive-oxidation path) or oxidized (via the oxidative-reduction path) at the electrode surface. This reagent reacts with the luminophore thereby aiding in the creation of the excited state [2,3].

Over time, ECL rapidly evolved from being a means of studying electron transfer reactions of organic molecules to an established analytical method, with successfully commercialized immunoassays [4–6]. In the last decade, ECL has further advanced into an imaging technique that allows the visualization of various objects [7], cells [8] and subcellular components [9] directly at the electrode surface [10–12].

The first single-molecule observation using ECL as measuring technique dates to 1995, when Wightman's research group reported the ECL annihilation reaction of 9,10-diphenylanthracene (DPA) in acetonitrile. A gold microelectrode was pulsed at approximately 1.8 kHz, inducing reversible conversion of DPA molecules to $DPA^{+\cdot}$ and $DPA^{-\cdot}$, which subsequently reacted with each other in the solution and generated excited states. To capture the emitted photons in the reaction layer, a photomultiplier tube (PMT) was placed approximately 2 mm from the surface of the microelectrode surface [13].

In contrast to traditional ECL detection utilizing a photomultiplier tube (PMT), ECL microscopy (ECLM) now employs a charge coupled device (CCD) to capture the ECL signal. The CCD is just a component of a comprehensive setup, which also includes a bright field microscope and an electrochemistry module, comprising an electrochemical cell and a

* Corresponding authors.
E-mail addresses: alessandra.zanut@unipd.it (A. Zanut), g.valenti@unibo.it (G. Valenti).

https://doi.org/10.1016/j.electacta.2024.144256
Received 9 December 2023; Received in revised form 7 April 2024; Accepted 8 April 2024
Available online 9 April 2024

potential generator. To minimize the luminescence loss during transmission, the distance between the sample and the CCD should be as short as possible. Moreover, mirrors or filters in the transmission pathway are recommended to be removed except for special applications. With advancements in electronic technology, electron multiplying charge-coupled devices (EMCCDs) have been combined with ECL technology to enhance imaging capabilities, allowing for higher-definition images and exploration of phenomena in the microscopic field [11]. However, EMCCD cameras are expensive and require a sophisticated optical path system, which has led to the development of innovative ECL imaging devices implemented in smartphones as image capturers, resulting in cost-effective solutions well-suited for the development of point-of-care testing (POCT) systems [14].

The ECL complex setup has been used to study primarily the heterogeneous mechanism of ECL, which involves the well-established Ru (II) Tris(2, 2′-Bipyridine)/ tri-*n*-propylamine ($[Ru(bpy)_3]^{2+}$/TPrA) dual system, operating in aqueous solutions. In this mechanism, the luminophore is linked to a sensing element, such as an antibody, a bead, or a DNA probe, which hinders its diffusion towards the electrode. As a result, ECL emission is initiated exclusively by the radicals produced through the anodic oxidation of TPrA ($TPrA^{\bullet+}$ and $TPrA^{\bullet}$) [2,3,15,16]. These radicals have limited lifetimes, which causes the ECL emission layer to be confined near the electrode surface, so, despite the extensive use of this heterogeneous mechanism, the visualization of objects located a few microns away from the working electrode remains an open challenge [15]. In this scenario, the synergy between ECL and microscopy has found applications across a wide spectrum, from discussing ECL mechanisms and limits to improving its use in biological contexts [17].

Marked by the emergence of various innovative material design, surface modification, and electrode architecture, this review collects different and original approaches for controlling the ECL active layer, with the goal of the advancement and refinement of ECLM.

2. Emitting layer in ECL systems

As previously stated, ECL remains localized in the proximity of the electrode surface, and the thickness of the ECL layer (TEL) is determined by the reaction intermediates. In annihilation ECL processes, the TEL is constrained by electrogenerated intermediates with shorter diffusion lengths, which are formed at one electrode. In the co-reactant ECL processes, the TEL differs based on the specific route taken. For the oxidative-reduction route and the low oxidation potential route, it is primarily dictated by the diffusion length of $TPrA^{+\bullet}$, while for the catalytic route, it depends on the diffusion length of $[Ru(bpy)_3]^{3+}$.

2.1. Tools for studying the emitting layer: ECLM

In this scenario, TEL measurement through ECL microscopy (ECLM) is key to deciphering ECL mechanisms and modifying the predominant co-reactant pathway [18]. ECLM now employs a comprehensive setup that includes a bright field microscope, an electrochemistry workstation that consists of an electrochemical cell and a potential generator, and a charge coupled device (CCD or EMCCD) to capture the ECL signal (Fig. 1a). Indeed, researchers indeed utilized ECLM to precisely control the ECL process by adjusting reactant concentrations [19–23]. This approach enabled precise imaging of cell-matrix adhesions and cell-cell junctions within the ECL layer, extending it several micrometers from the electrode surface [21] mainly in static [22] but also in dynamic conditions [24,25]. Beyond examining the spatial distribution of excited luminophores, other investigations involved analyzing co-reactant radicals near the electrode surface [5] to address challenges related to co-reactant lifetime and slow mass transport. As researchers tried to uncover the underlying ECL mechanisms and optimize co-reactant pathways, the experimental setup of ECLM served as a critical tool for measuring the thickness of the ECL layer (TEL).

One limitation of this technique is that, restricted by the optical diffraction limit, ECLM is not suitable for measuring TEL smaller than approximately 200 nm [26]. In contrast, scanning electrochemical microscopy (SECM) allows precise control of the distance (<100 nm) between the tip and substrate, making it capable of investigating co-reactant radicals with short lifetimes [18].

2.2. Tools for studying the emitting layer: SECM-ECL

Scanning electrochemical microscopy (SECM) is a scanning probe

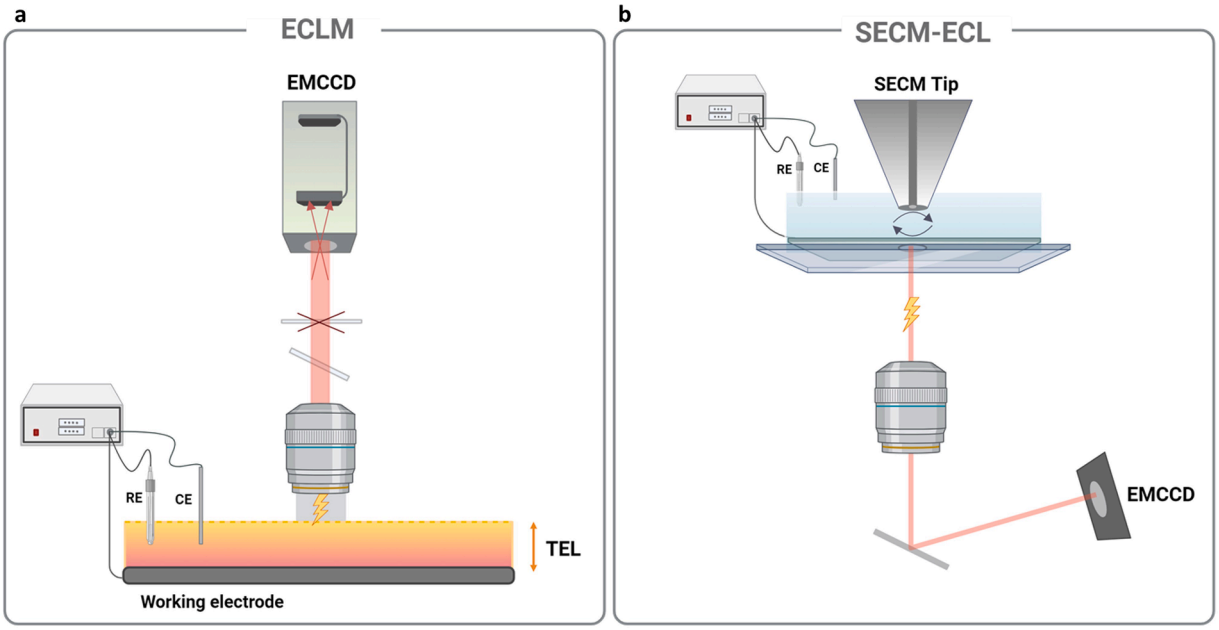

Fig. 1. (a) Schematic representation of ECLM that includes an electrochemical cell, a microscope objective, and a charge coupled device (EMCCD) to capture the ECL signal. (b) Schematic representation of SECM-ECL, including a small-scale probe (SECM-tip), an inverted microscope objective, and a charge coupled device (EMCCD) to capture the ECL signal.

technique where a small-scale electrode scans across an immersed substrate, simultaneously recording the current response. This response is based on both the surface topography and the electrochemical activity of the substrate. The strength of SECM lies in its ability to precisely quantify material flux from a surface with exceptional spatial and temporal resolution.

A typical SECM setup comprises a small-scale probe, often on the micrometer to nanometer scale (referred to as a SECM tip), connected to a low-current bipotentiostat (≤pA) (Fig. 1b). This setup allows for precise measurement and control of current and potential at the probe and substrate interfaces. The tip's movement is facilitated by a high-resolution three-dimensional (3D) positioning system, utilizing an x, y, and z stage equipped with stepper and piezoelectric motors for coarse and fine adjustments, respectively.

Advancements in understanding the mechanisms of ECL have been achieved by integrating ECLM with SECM. This was possible due to the integration of a photomultiplier tube (PMT) within a SECM setup, which is mounted on top of an inverted microscope, enabling enhanced visualization and analysis.

Based on SECM-ECL experiments, Miao et al. validated the so-called low oxidation potential mechanism of $[Ru(bpy)_3]^{2+}$/TPrA system, in which the diffusion length and half-life of $TPrA^{+\bullet}$ was estimated with the help of digital simulations [15]. They investigated the ECL distribution in the proximity of the electrode (≥1 μm) surface controlling the distance between a hemispherical microelectrode and the electrode surface using a micromanipulator. Expanding from this, our group investigated the ECL efficiency at very short distances (≤1 μm) using a transparent indium tin oxide (ITO) electrode functionalized with a $[Ru(bpy)_3]^{2+}$ monolayer as the emitting surface. Two different hemispherical Pt microelectrodes (diameter of 1.5 or 0.5 mm) for TPrA oxidization were positioned on an inverted microscope equipped with an EMCCD camera. This system was coupled with a micropositioner to precisely control the tip-substrate distance. This approach combined with the use of labeled microbeads, revealed the contribution of an additional pathway to ECL generation 10 times more intense than the signals measured at larger distances (>1 μm) [5].

In another study, Lopez et al. studied the distance dependence of ECL emission from $[Ru(bpy)_3]^{2+}$ and rubrene as a model to provide information on the kinetics, stability, and mechanism of the light emission process. To this aim, they tuned the distance between the SECM tip (cathode) and a transparent microsubstrate (anode) measuring the concurrent steady-state generation of radical ions.

They observed that reducing the tip-substrate distance enhanced ECL intensity, allowing them to create light approach curves for precise tip positioning. Intriguingly, ECL was detected before the electrochemical reduction of $[Ru(bpy)_3]^{2+}$ or rubrene during cyclic voltammetry at the tip. This was attributed to inverse photoemission, where radical cations formed on the substrate transferred holes to the tip and external power sources injected electrons into the tip, resulting in light emission [27]. Recently, Zhou et al. used SECM to demonstrate the enhancement effect of silica nanochannel membranes (SNM) on ECL generation by $[Ru(bpy)_3]^{2+}$/TPrA. This enhancement was attributed to SNM's negatively charged ultrasmall nanochannels, which enrich and electrostatically attract the species. Furthermore, by measuring the SECM approach curve measurements in conjunction with using finite element simulations, they were able to quantitatively measure the mass transfer rate of $[Ru(bpy)_3]^{2+}$ within the channels of SNM (ca. 0.3 mm/s) finding a much faster rate than that in the bulk solution [28].

3. Control strategies for the emitting layer

3.1. Novel reagents and material design

Although ECL demonstrates impressive spatial resolution, it is essential to expand the thin ECL layer beyond the electrode surface. This expansion is currently constrained by the relatively short lifetime of electrogenerated co-reactant radicals. In this context, the significance of the luminophore cannot be emphasized enough. Traditionally, ECL emitters have been categorized into inorganic and organic probes based on their functional components. Recently, the easy functionalization and favorable biocompatibility have made organic molecules promising candidates for ECL applications. Since its first study in 1928 [29], luminol has emerged as the leading organic ECL luminophore. This is attributed to its nontoxicity, low oxidation potential, and considerable ECL signal when combined with exogenous co-reactant H_2O_2. The mechanism governing luminol's ECL closely resembles that of chemiluminescence [30] whereby the anion of luminol generates diazaquinone through single electron transfer at the electrode. Then it is further oxidized by a superoxide radical or hydrogen peroxide anion to a 3-amino-o-dicarboxylate anion. After that, luminol returns to the ground state, accompanied by light radiation [31].

Hu et al. selectively electropolymerized luminol on an indium tin oxide (ITO) electrode after applying a sebaceous fingerprint. The inert components of the fingerprint reduced the electrochemical activity in specific electrode regions. Cyclic voltammetry (CV) allowed the electropolymerization, resulting in a polyluminol film whose thickness affected current peaks. After the third CV cycle, the current signals decreased due to a hindrance in mass transport and charge transfer at the ITO electrode caused by the higher thickness of the polyluminol film. The reduction in current was attributed to redox transformations of polyluminol involving ion transport through the film. This process produced recognizable negative fingerprint images captured using a CCD camera applying a constant 1.2 V potential with a 100-second exposure time [32].

In contrast to other visualization technologies, this method stands out for its simplicity and minimal reliance on complex instruments. However, the unstable ECL emission of luminol, caused by the self-decomposition of H_2O_2, has led to the exploration of alternative approaches. In this context, dissolved dioxygen (O_2) has emerged as a promising substitute for H_2O_2 due to its low toxicity and inherent stability [33]. However, the luminol-O_2 system suffers from an ultralow ECL signal due to the inefficient production of reactive oxygen species (ROS). Despite efforts to enhance ECL signals through nanomaterials [34] or ultrasound [35], the limitations of poor solubility of organic molecules and their dependence on annihilation reactions have limited their application in ECLM [36].

Unlike organic molecules, inorganic ECL probes, including coordination complexes such as $[Ru(bpy)_3]^{2+}$ and its derivatives, as well as Ir (III) complexes [37] and multicolor complex luminophores [38] are widely employed in chemical analysis. These probes offer advantages such as tunable wavelengths, high efficiency, and excellent stability in aqueous solutions [39]. Frequently, instead of directly incorporating them into the ECL system detection solution, they are commonly immobilized on the surface of an electrode and coupled with sacrificial co-reactants [40]. However, a substantial drawback in this scenario lies in the notable reduction in ECL intensity over time, which stems from the diffusion of co-reactant radicals over short distances away from the electrode surface. To overcome this limitation, many efforts have been made in recent times, also extending the focus beyond the luminophore. By combining ECL and microscopy, and the use of labeled microbeads (called Ru@beads because beads are labeled with $[Ru(bpy)_3]^{2+}$), for example, our group mapped the ECL generation close to the electrode surface (≤1 μm) and identified a mechanism for boosting ECL emission by optimizing the distribution of radicals and luminophores. We introduced the branched amine N-dipropyl isobutyl amine (DPIBA), as additive to generate a stable carbocation, increasing the efficiency of C–N cleavage, i.e., the efficiency of the pathway at short distances. Based on the proposed mechanistic hypothesis, 50 mM of DPIBA was introduced as additive during ECL generation obtaining a signal increase of 66 % at the single bead level compared to TPrA. Moreover, an even more substantial signal enhancement of 128 % was observed at small distances, specifically when employing 0.3-μm Ru@beads with 30 mM DPIBA,

further confirming the higher reactivity at short distances [5]. Bin su and co-workers further investigate the generation of ECL by $[Ru(bpy)_3]^{2+}$ and five other tertiary amine co-reactants by combining electrochemiluminescence (ECL) self-interference spectroscopy and microscopy imaging, finding that 2,2-bis(hydroxymethyl)−2,2′, 2″-nitrilotriethanol (BIS-TRIS) can well balance the trade-off of distance reactivity of ECL and enhance the sensitivity by 236 % compared to TPrA in the bead-based immunoassay of carcinoembryonic antigen [41]. Employing labeled microbeads, Fiorani et al. demonstrated the ability to adjust the TEL by modifying the buffer capacity. When increasing the PB concentration from 0.01 M to 1 M, the TEL was reduced from 3.1 μm to 2.4 μm. A higher concentration of PB results in an increased presence of phosphate ions for buffering H^+ produced from $TPrA^{+\bullet}$ deprotonation, thereby facilitating the deprotonation process. This, in turn, leads to a shorter diffusion length of $TPrA^{+\bullet}$ and a smaller TEL [17].

In the same year, in response to the urgent need to transport co-reactant to emitter and the short lifetime of the radicals, Wang et al. designed a dual intramolecular electron transfer strategy and tertiary amine conjugated polymer dots (TEA-Pdots) as a co-reactant embedded ECL mechanism and microimaging system. To improve the performance of co-reactant embedded Pdots, two types of anodic co-reactants were coupled to the backbone of poly[(9,9-dioctylfuor-enyl-2,7-diyl)-alt-co-(1,4-benzo-{2,1,3}-thiadiazole)] (PFBT) resulting in the creation of diethylamine-conjugated PFBT (TEA-PFBT) and dipropylamine-conjugated PFBT (TPA-PFBT). TEA-Pdots stood out showing an ECL efficiency 132 and 45 times stronger than those of the mixture of Pdots with TEA at equivalent and 62.5 times higher amounts, respectively. The efficiency of ECL was even higher than that of a typical $[Ru(bpy)_3]^{2+}$ system. This strong ECL emission was attributed to fast intramolecular electron transfer, which significantly enhances the ECL emission by shortening the electron transfer pathway and reducing the complexity of transporting radical intermediates in intermolecular electron transfer

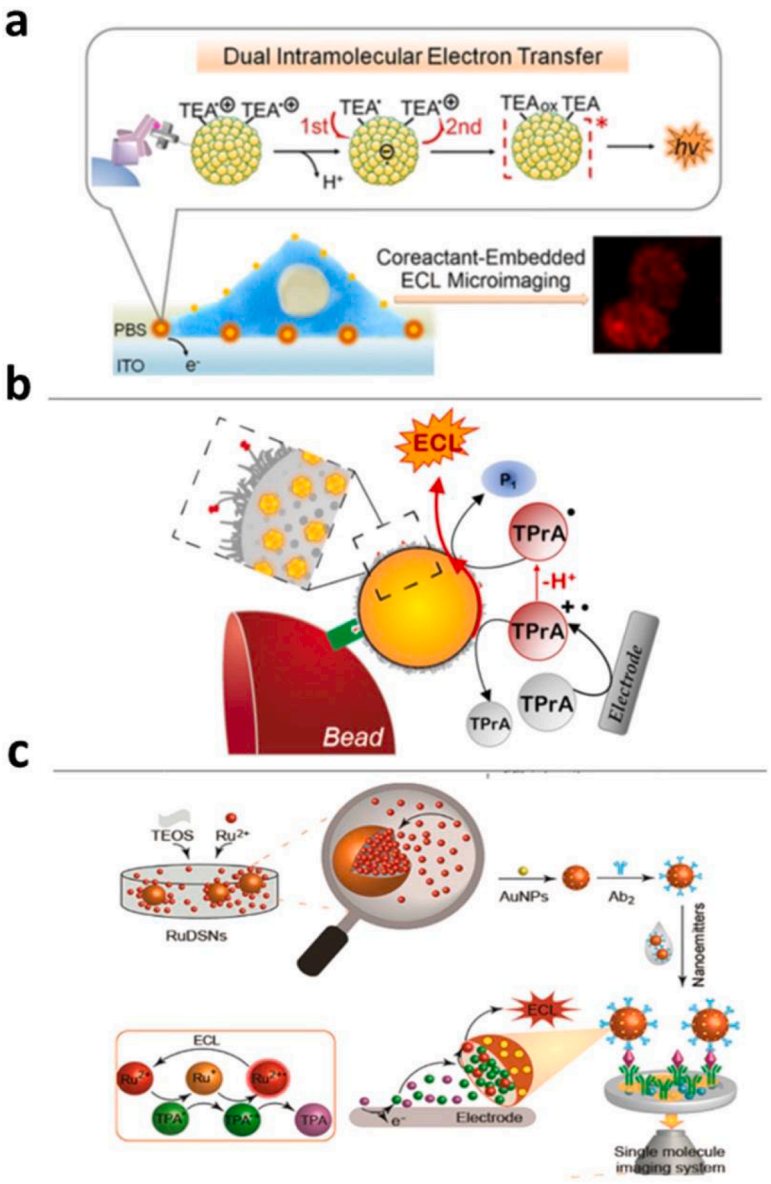

Fig. 2. (a) Schematic representation of the proposed co-reactant-embedded ECL mechanism and microimaging system with tertiary amine conjugated polymer dots (TEA-Pdots). Reproduced from Ref. [42]. with permission from Angewandte Chemie International Edition © 2020 Wiley-VCH GmbH. (b) The heterogeneous mechanism for the generation of co-reactant ECL 'oxidative reduction' obtained using 2.8 mm beads labeled with bio-Triton@RuNp (yellow sphere) through a streptavidin (green tool)-biotin (red tool) bond. Reproduced from Ref. [47]. with permission from Angewandte Chemie International Edition © 2020 Wiley-VCH GmbH (c) Schematic illustration of RuDSN/AuNPs labeled with monoclonal antibodies single-protein-molecule imaging by ECL. Reproduced from Ref. [12] with permission of Copyright © 2021 American Chemical Society.

-based ECL processes. This enhancement, along with the negligible cytotoxicity of TEA-Pdots, led to interesting applications of the microimaging system in the visual analysis of membrane proteins in single living cells and the *in situ* evaluation of their expression change after drug treatment (Fig. 2a) [42].

More recently (2022), Han et al. introduced $[Ru(bpy)_3]^{2+}$-functionalized microgels (Ru-MGs) to decorate polystyrene beads (called Ru-MG@bead) as a strategy to extend the size of the ECL-emitting layer. Ru-MGs were synthesized by an aqueous polymerization of free radical precipitation with the complex $[Ru(bpy)_3]^{2+}$ successfully grafted to the poly(N-isopropylacrylamide) hydrogel matrix (pNIPAM). Efficient labeling and stable emission of the Ru-MG@bead were imaged by both top- and side-view configurations. Remarkably, the ECL intensity of Ru-MGs@beads showed a 9-fold enhancement compared to beads functionalized by a sandwich immunoassay or an amide bond. This improvement was attributed to the higher density of ruthenium sites on the beads located in close proximity to the electrode surface. These Ruthenium sites underwent direct oxidation, which contributed more effectively to overall ECL signals [43].

Recent years have also witnessed the coupling of ECL to nanotechnology to advantageously be used as ECL-active systems. The first instance of nanomaterial-generated ECL dates back to 2002, when Bard and colleagues employed semiconductor silicon nanocrystals (NCs) to produce ECL via both annihilation and co-reactant mechanisms in acetonitrile solutions [44]. Afterward, Dye-doped silica nanoparticles (DDSNs) were used to study and optimize the ECL emission performances by varying their physical−chemical properties. In 2009, Zanarini et al. demonstrated the remarkable chemical and electrochemical stability of $Ru(bpy)_3$ incorporated in DDSNs and to maximize the emission as a function of DSNP size, doping material, charge, doping level, supporting electrolyte, electrode material, and solvent buffers [45]. A subsequent study revealed that the effectiveness of ECL generation in covalently doped $[Ru(bpy)_3]^{2+}$ core-shell silica-PEG nanoparticles is mainly influenced by the doping level. In fact, they demonstrated the presence of two distinct mechanisms that govern the generation of ECL, which are influenced by the density of the dye and the overall charge of the nanoparticles, since the latter can influence the distribution of charged species involved in the ECL process within and around the nanoparticles [46].

This issue is mainly due to several limitations related to the synthetic strategy adopted for DDSNs. Starting from this, Zanut et al. introduced a novel family of DDSNs, named bio-Triton@RuNPs, synthetized by a reverse microemulsion method that enabled a high degree of dye doping (approximately 4800 complexes per NP) without resulting in a positive surface charge, thus allowing for a strong ECL emission. Using TPrA as a co-reactant, these DDSNPs exhibited a remarkable enhancement in ECL signal compared to the conditions mimicking commercial ECL-based immunoassay systems, which usually rely on antibodies labeled with six dyes (Fig. 2b) [47].

Liu et al. introduced an alternative strategy for improving the performance of RuDSNPs, involving the integration of gold nanoparticles to form RuDSNs/AuNPs nanoemitters. In this case, the ECL emission is confined to the local surface of RuDSNs leading to a twofold increase in ECL emission. When these nanoemitters were used in conjunction with TPA as a sacrificial co-reactant, their effectiveness was demonstrated in successfully visualizing both individual protein molecules at the electrode and cellular membrane proteins [12]. Briefly, RuDSN/AuNPs labeled with monoclonal antibodies against cytokeratin 19 (CK19) proteins were introduced to form sandwich immuno complexes on an ITO electrode (Fig. 2c). In contrast to the wide-field fluorescence microscopy, the ECL images showed near-zero background, resulting in a high signal-to-noise (S/N) ratio for proteins' visualization. However, the limited accessibility of reaction intermediates to $[Ru(bpy)_3]^{2+}$ within RuDSN/AuNPs posed a challenge, causing significant leakage of $[Ru(bpy)_3]^{2+}$ and resulting in a decrease in luminescence during continuous imaging. In response, the same research team shifted their focus to porous nanomaterials designing $Ru(bpy)_3^{2+}$ embedded metal-organic frameworks complex (RuMOFs) through solvothermal reaction. Notably, compared to surface-modified/dye-doped nanomaterials such as RuDSN/AuNPs, the unique multipore confined space within the MOF design increased the reaction sites for $[Ru(bpy)_3]^{2+}$ with TPrA. This enhancement led to more efficient electron/proton transfer, resulting in amplified photon generation efficiency. By employing single RuMOFs to label individual proteins in living cells, they were able to visualize the distribution of membrane tyrosine-protein-kinase-like7 (PTK7) proteins in cells with low expression levels using ECL on an ITO electrode. It is worth noting that these ECL nanoemitters, characterized by their exceptional confined-specific surface area and porosity, greatly enhanced the accumulation of intermediate radicals, extending ECL emission duration to up to 1 h [48].

As emerged, a wide range of nanomaterials can serve as versatile platforms for enhancing ECL signals. Rebeccani et al. proposed the use of Ru-functionalized carbon nanotubes (CNT-Ru) as efficient nanomaterials to optimize the distribution of the ECL-emitting layer [49]. Carbon nanotubes can create a conductive layer around the beads, extending the ECL active layer and enhancing the ECL signal through the direct oxidation of the luminophore on this new conductive layer. The latter mechanism is not active in a conventional bead system, in which direct oxidation of the luminophores is neglected. To validate the boosting effect of CNT, the authors functionalized micromagnetic beads with CNT-Ru through a strong biotin-streptavidin bonding (beads@CNT-Ru) and imaged them on platinum electrodes. The ECL emission was compared to that of standard 2.8 mm microbeads functionalized with a biotinylated antibody labeled with $Ru(bpy)_3^{2+}$ complex (beads@Ru) showing a significant increase of approximately four-fold, suggesting that CNTs played a strategic role in improving the ECL signal.

The combination between carbon-based nanomaterials and ECL is due to other unique and advantageous mechanisms, such as the so-called "Wavelength-Tunable Electrochemiluminescence". Yang et al. reported a facile way to modulate the ECL wavelength of carbon dots (CDs) in an aqueous solution by phosphorus (P) doping. As a result, the ECL wavelength was finely tuned from 425 to 645 nm solely by adjusting the concentration of P dopants; meanwhile, the ECL efficiency, determined by the ratio of the generated photon number per consumed electron relative to the $[Ru(bpy)_3]^{2+}/K_2S_2O_8$ standard, was increased more than 5-fold maximum. This was possible because P doping in PNCDs could reduce the surface-deep electron-trapping state, promote the electron–hole separation, and enhance the electron conductivity, all of which boosted the ECL performance of PNCDs [50].

The development of wavelength tunable ECL offers the potential for achieving the long-standing challenge of real-time dynamic observation of biomolecules through ECL imaging. Wang et al. utilized ECL nanoemitters composed of CdZnSeS quantum dots (QDs) and glucose oxidase (GOx) to monitor the movement of wheat germ agglutinin (WGA) on cell membranes. The ECL signals of QD-WGAs weakened over time due to the consumption of H_2O_2, while the ECL signal of QGP-WGA remained stable. Using a 2D Gaussian fitting method, they precisely located individual spots and reconstructed movement trajectories of each particle on the cell membrane. Dual-color single particle tracking (SPT) based on ECL imaging was employed to investigate dynamic interactions between WGA and cholesterol. Overall, the study showcased the potential of the developed system for multicolor SPT based on ECL imaging, facilitating real-time observation of dynamic biomolecular interactions on cell membranes [51].

3.2. Strategies to modulate charge transfer

As emerged, the conventional "oxidative-reduction" ECL pathway, based on freely diffusing co-reactant radicals, faces a difficulty due to the short lifetimes of most common radicals. This problem becomes particularly critical for intracellular studies as the radical must penetrate the cell [52]. In addressing this challenge, the advancement of ECL

microscopy has been propelled by a sequence of groundbreaking investigations. Recent findings indicate that the imaging potential of ECL microscopy can be substantially enhanced by regulating the proportional contributions of various ECL pathways [19]. Ding et al. introduced a strategic approach that effectively modulates the ECL reaction pathway by varying the concentration of luminophore and/or co-reactant (Fig. 3a). This strategy allowed sequential and selective imaging of cell–matrix adhesions and cell–cell junctions in a single sample by extending the ECL layer several micrometers away from the electrode surface. To clarify, at low concentrations of $[Ru(bpy)_3]^{2+}$, ECL was confined to the electrode surface, revealing cell-matrix adhesions at the bottom of the cell. A higher $[Ru(bpy)_3]^{2+}$ concentration thickened the ECL layer, allowing sequential imaging of both cell-matrix adhesions and cell-cell junctions through the catalytic route [20]. Expanding on this concept, Ma et al. exploited the potential of the catalytic route to realize the ECL imaging of intracellular structure and dynamic transport. They employed $[Ru(bpy)_3]^{2+}$ as a molecular antenna to connect extracellular and intracellular environments, while making use of intracellular biomolecules as co-reactants. Applying a constant 1.3 V to an ITO electrode in the presence of freely diffusing $[Ru(bpy)_3]^{2+}$ solution resulted in the electro-oxidation of $[Ru(bpy)_3]^{2+}$ to $[Ru(bpy)_3]^{3+}$, forming a diffusion layer in the vicinity of ITO surface. This $[Ru(bpy)_3]^{3+}$ diffusion layer exhibited a thickness of 10 μm within the initial 10 ms, gradually expanding over time (where $\delta = 4\sqrt{Dit}$, with δ representing the diffusion thickness, Di as the diffusion coefficient [6.0 × 10–6 cm^2/s], and t indicating the duration of voltage). In addition, intracellular amine-rich biomolecules exhibited distinct enhancement factors, which facilitate the imaging of hierarchical intracellular structures such as the nucleolus, nucleus, and endoplasmic reticulum without employing multiple labels [21].

Similarly, catalytic route ECLM evolved to visualize cell membranes using nitrogen-doped carbon dots (NCDs) as the nano co-reactants. To endow NCDs with recognition capacity, polystyrene binding peptides (PSBP) were modified on NCDs to target the phosphatidylserine (PS) on the membranes of apoptotic cells. The ECL emitting layer was extended due to the long lifetime of electro-oxidized $[Ru(bpy)_3]^{3+}$. Furthermore, amine-rich NCDs as highly efficient nano co-reactants contributed to a substantial increase in ECL intensity (by a factor of 245) allowing the z-scanned serial ECL images of upper cell membranes [22].

A novel approach was adopted by Meg et al. which exploited temperature as a means of transition from one ECL pathway to another. They developed a temperature tuned ECL layer by coupling a digital heater plane to the nonconductive side of an ITO electrode to record the evolution of shadow regions of adherent cells. Finite element simulation and experimental results demonstrate that the thickness of the ECL layer (TEL) is reversibly regulated by electrode temperature (Te), so that single cell topography at different heights has been imaged. The TEL shows different regulation ranges as a function of Te in two ECL routes, the homogeneous and catalytic one. At a high concentration of $[Ru(bpy)_3]^{2+}$, the catalytic route depending on the diffusion of $[Ru(bpy)_3]^{3+}$ allows an obvious extension of the TEL from the bottom of the cell to the top. This approach enabled the section imaging at different heights of the cell by subtracting images at adjacent Te. On the other hand, the ECL layer in the oxidative reduction route is confined to the electrode surface and shows moderate extension with elevated Te [23].

The rapid progress of ECLM is not only attributed to changes in the ECL pathway through catalytic processes. The interplay between the classic Positive ECL (PECL) and the relatively new Shadow ECL (SECL) has also been exploited to obtain complementary information about the imaged object (Fig. 3b). As already mentioned above, the PECL approach utilizes $[Ru(bpy)_3]^{2+}$ to mark cellular membrane proteins enabling visualization of protein expression, membrane transport, and surface-associated processes directly at the electrode surface. Conversely, SECL exploits the hindrance of ECL reagents diffusion by cellular structures, resulting in dark regions (shadows) corresponding to those structures. SECL has been applied to the study of single cells with remarkable spatial resolution, cell-matrix adhesions, morphological changes under oxidative stress, migration of living cells, and imaging mitochondria [53]. In particular, in 2021, Ma et al. introduced an effective SECL approach based on the use of freely diffused $[Ru(bpy)_3]^{2+}$ dye and the highly efficient sacrificial TPA co-reactant. This homogeneous setup allowed the visualization of individual mitochondria, an achievement that proved challenging using conventional fluorescence methods [54]. In a subsequent development, the same research group enhanced SECL demonstrating the imaging of single cells and organelles with micrometric resolution under ultrasensitive conditions. Their

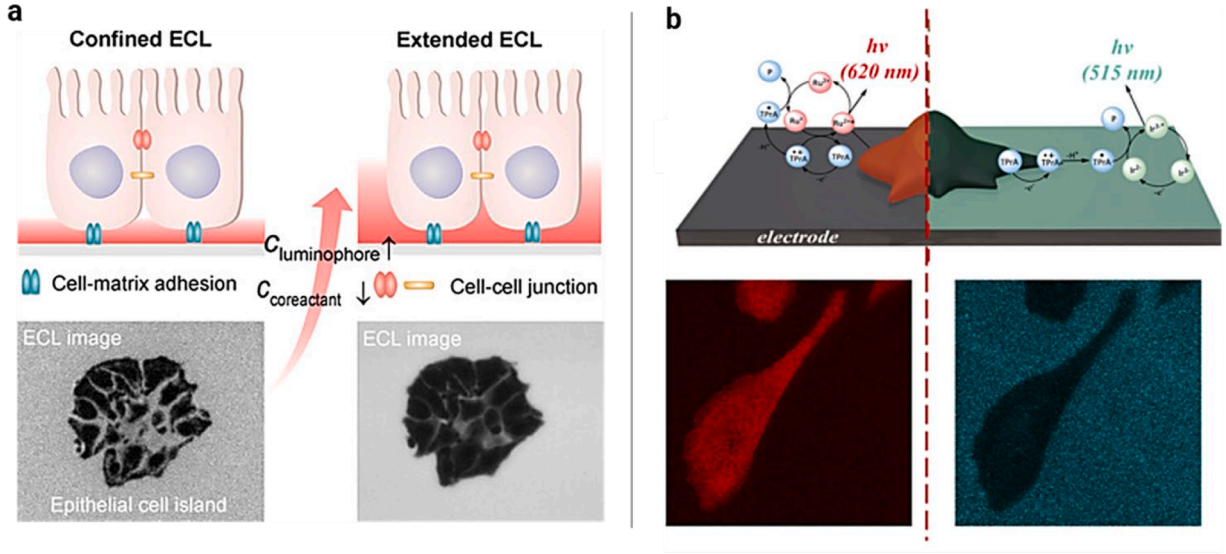

Fig. 3. (a) Controlling ECL Layer Thickness for Selective Cell-Junction Imaging. Modulating luminophore and co-reactant concentrations enables precise adjustment of the ECL layer thickness, facilitating spatially selective imaging of cell-matrix adhesions and cell-cell junctions. Reproduced from Ref. [20] with permission from Angewandte Chemie International Edition. (b) Positive and Shadow ECL. Schematic representation of multimodal imaging of a cell immobilized on a glassy carbon electrode. Mechanism of co-reactant PECL (heterogeneous route involving mainly dissolved TPrA and SA@Ru label immobilized on the cell) and SECL (homogeneous route involving only dissolved $[Ir(sppy)_3]^{3-}$and TPrA) modes. Single CHO-K1 cell was imaged by PECL, and SECL. Reproduced from Ref. [53] with permission from Copyright © 2023 American Chemical Society.

label-free method was based on the extreme dilution in space of the luminophore and on the diffusional hindrance of the ECL reagents by the biological entities deposited on the electrode surface. Thus, the sharp negative ECL contrast images, acquired using the Electron Multiplication (EM) mode of an EMCCD camera, were generated at nanomolar and picomolar concentrations of luminophores, nearly seven orders of magnitude lower than conventional practices [55].

Following the same principles, Zhou et al. developed a new tunable ECL imaging mode that can switch from the negative contrast ECL imaging without labeling to positive contrast ECL imaging through the adsorption of $[Ru(bpy)_3]^{2+}$ for bacterial imaging. Bacterial cell walls are mostly negatively charged and can absorb positively charged luminescent molecules. Exploiting this characteristic, they were able to image E. coli and S. aureus species by tuning PB buffer and $[Ru(bpy)_3]^{2+}$ concentrations and keeping DBAE constant. In particular, changes in bacterial imaging contrast based on $[Ru(bpy)_3]^{2+}$ concentration exhibited specificity depending on the type of bacteria [56]. While the label-free method provided by SECL is attractive and avoids problems associated with PECL, such as its relatively weak luminescence and the fading of the ECL signal over time, it is unable to differentiate between processes taking place on or inside the cellular membrane, nor can it distinguish between proteins or various biological factors in different cells. This prompt Kezevic and colleagues to develop a bimodal approach that combines PECL and SECL. They exploited the simultaneous emissions of $[Ru(bpy)_3]^{2+}$ used to label the cellular membrane (PECL) and $[Ir(sppy)_3]^{3-}$ dissolved in solution (SECL). Their unique emission wavelengths (620 nm for $[Ru(bpy)_3]^{2+}$ and 515 nm for $[Ir(sppy)_3]^{3-}$) allow for straightforward spectral resolution by employing appropriate emission filters. Furthermore, when the two ECL modalities capture the same region of interest within a cell, the area emits ECL intensities at different wavelengths, thus offering complementary information. While PECL imaging reveals the distribution of Ru labels on the cell membrane, SECL provides insight into the hindrance of ECL reagent diffusion caused by the cell membranes. However, due to the low co-reactant ECL efficiency of $[Ir(sppy)_3]^{3-}$, the intensity of the SECL signal is relatively low. Therefore, the next step in this investiogation would involve replacing this luminophore with similar Ir(III) complexes that offer a higher ECL intensity [53].

3.3. ECL imaging based on bipolar electrochemistry to modulate co-reactant lifetime and mass transport

The emergence of new analysis equipment, the variety of nanomaterials available, and the mastery over various ECL pathways has promoted the development of high-resolution ECL imaging technology. These advances, when coupled with innovative micro/nano devices and bipolar electrochemistry, have opened new avenues for addressing challenges associated with co-reactant lifetime and slow mass transport [57]. Essentially, micro/nano fabricated electrochemical devices offer precise control over geometry, effectively limiting reaction volumes to these minute dimensions, resulting in a significant enhancement of the electrochemical signal [58]. Bipolar electrodes (BPEs) have the potential advantage of being able to miniaturize [39]. In this setup, a BPE serves as an electronically conductive element in contact with an ionically conductive phase. Under a sufficiently high electric field across the ionic phase, faradaic reactions occur at the BPE ends, even without a direct connection to an external power source. This wireless setup is unconventional as the potential difference is determined by the electric field in the solution. Despite this reversal, control over the difference in interfacial potential is maintained [59,60].

Although the synergy between microfabricated BPE and ECL offers several benefits, there are some notable drawbacks that may be recognized. First, addressing micrometric or nanometric objects by BPE represents a difficult task, because it requires high electric fields for polarization. Moreover, limited sensitivity is attributed to the tiny sample volumes employed. To address these challenges, researchers have proposed various strategies. Voci et al. for instance elaborated a solid-state micropore decorated with a rhombus-shaped gold microelectrode. The electric field strength was concentrated inside the solid-state micropore where the conductive gold microelectrode was precisely located and acted as a bipolar light-emitting device. This original configuration allowed for adequate polarization of the gold microelectrode in a wireless manner, which locally led to ECL emission [61]. On the other hand, optimizing the distance between electrodes and selecting suitable materials emerged as an effective strategy to enhance sensitivity. In this regard, Anderson et al. fabricated a massive array of closed bipolar ultramicroelectrodes (UMEs) to imaging highly dynamic redox processes. The fabrication involved creating a carbon array on a Si substrate, which was then insulated using parylene C. The arrangement was designed in a hexagonal pattern to optimize electrode spacing and density. The resulting device was used to study the generation, diffusion, and depletion of $Fe(CN)_6^{3-}$ on an Au UME. By applying +0.8 V oxidizing potential, they produced $Fe(CN)_6^{3-}$ through $Fe(CN)_6^{4-}$ oxidation, resulting in a larger illuminated zone expanding to approximately 400 μm within 2 s. However, after 3 s, the center's intensity decreased, forming a dark depletion zone under the Au UME position. At the outset, the spatial resolution was found to be limited by the size of the bipolar UMEs and their spacing. This limitation could potentially be addressed by reducing electrode dimensions and interelectrode spacing. Conversely, the temporal resolution was limited only by the data transfer rate of the camera [62]. Expanding on the accomplishments of Anderson et al., Iwama and coworkers used a closed BPE (cBPE) array, fabricated via electroless plating on a micropore membrane, to image the respiratory activity of MCF-7 spheroids with high spatio-temporal resolution (Fig. 4). The initial phase involved monitoring the flow of $[Fe(CN)_6]^{3-}$ on the cBPE with a CCD camera. The ECL signals conjugated to the reduction of $[Fe(CN)_6]^{3-}$ molecules reflected the spreading activity of $[Fe(CN)_6]^{3-}$ on the BPE array on the sample chamber side. Subsequently, an evaluation of the oxygen consumption of MCF-7 was carried out using bipolar ECLM (BEM), which revealed a noticeable reduction in the surrounding ECL spheroids as a result of oxygen consumption. This BEM methodology offered improved spatial resolution, providing 2D insights into cell respiration compared to traditional methods [63]. However, a common element in both recent studies is the incorporation of an initial assessment to evaluate the consistency of the potential and ECL response. This step is essential because the cell geometry greatly influences the distribution and strength of the potential gradient generated on the surface of the bipolar electrode (BPE), and monitoring this process is challenging due to the wireless nature of the BPE.

Interestingly, Villani et al. map the potential gradient in bipolar electrochemical cells with different geometries that exploit the stable ECL signals generated through luminol/H_2O_2. In a linear bipolar arrangement, the potential of the BPE varies uniformly across its surface, allowing the expansion of the ECL area by increasing the applied total voltage (E_{tot}). When configured as a cylinder, the anodic potential gradient on the BPE's surface transitioned from a spot to a ring-like shape with rising values of E_{tot}. Utilizing a single BPE in a U-type electrolytic cell primarily generated ECL emission on the cathode side. As E_{tot} increased, the ECL region expanded towards the center until reaching a shielding wall. However, employing a pair of BPEs resulted in an asymmetric ECL emission pattern, accentuated at higher E_{tot} values as a result of the floating potential of the BPE adjusting to the solution potential. Conversely, electrically connecting the two BPEs using an ammeter transformed the asymmetrical ECL emission into a single, uniform ECL emission region, aligning with the pattern observed with a single BPE [64].

In addition to the uniformity of the ECL response, another critical aspect involves the choice of the electrode and the deliberate control of the electric field's focus and shape. This constitutes a notable and effective strategy for improving the efficiency of bipolar electrochemical and ECL cells. Subsequently, Douman et al. created a wireless ECL system based on 3D-printed titanium arrays as feeder electrodes and gold

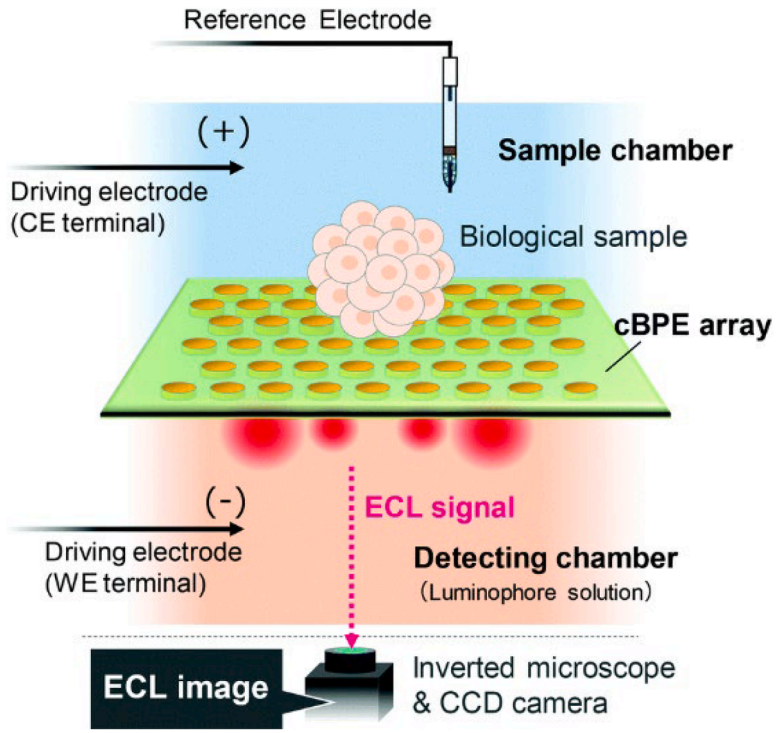

Fig. 4. Schematic illustration of BEM. Reproduced from Ref. [63] with permission of the royal society of chemistry.

microparticles (45 lm diameter), functionalized with 11- mercaptoundecanoic acid, as microemitters. These titanium arrays, created using selective laser melting, produced intense electric fields whose distribution depends on the geometry of the array, enabling conductive microparticles as individual bipolar electrodes and localized ECL. Using [Ru(bpy)$_3$]$^{3+}$ and TPA, Au microparticles generate ECL at a minimum electric field strength, and the intensity increases until it levels out as the field strength increased. This behavior aligns with the influence of heterogeneous electron transfer across the titanium oxide layer on ECL generation. Furthermore, the use of charged microparticles as a massively parallel array of bipolar electrodes enhanced ECL through electrokinetic transport, facilitating the entry of more particles into the ECL generation zone per unit of time [65].

4. Summary and outlook

This review focuses on recent advancements in controlling the electrochemiluminescence (ECL) active layer, with the ultimate goal of refining ECL microscopy (ECLM). Notably, the utilization of scanning electrochemical microscopy (SECM) has allowed for precise control of the distance between the tip and substrate, facilitating the study of the thin ECL layer (TEL) at a resolution below 200 nm. Strategies for improving TEL, in conjunction with ECL imaging, involve optimizing luminophore performance and introducing new co-reactants to enhance radical diffusion close to the electrode surface. Recent developments have witnessed the integration of ECL with nanotechnology, leading to the creation of novel dual-doped silica nanoparticles (DDSNP), nanoemitters, and carbon materials. These innovations demonstrate superior capabilities in efficiently transporting co-reactant radicals to the luminophore, thereby enhancing the ECLM readout. However, challenges persist, particularly in addressing the short lifetimes of common radicals and ensuring effective intracellular studies. The evolution of ECL microscopy has been further enhanced by the regulation of different ECL pathways to significantly enhance imaging potential. Exciting progress has been made possible by the introduction of advanced analytical equipment, diverse nanomaterials, and a comprehensive understanding of various ECL pathways. The integration of innovative micro/nano devices and bipolar electrochemistry has paved the way for addressing challenges related to co-reactant lifetime and slow mass transport. Although the combination of microfabricated bipolar electrodes (BPE) with ECL has demonstrated remarkable effectiveness, the complex and time-consuming fabrication process for high-density BPE arrays remains a persistent challenge. Overcoming this obstacle necessitates streamlining the fabrication steps for the creation of multiple electrode systems, especially in the context of performing multiplex assays. Despite these challenges, the continued integration of cutting-edge techniques holds promise for further advancements in the field of ECL microscopy.

Declaration of competing interest

The authors declare the following financial interests/personal relationships which may be considered as potential competing interests:

Giovanni Valenti reports financial support was provided by Ministry of Education and Merit. If there are other authors, they declare that they have no known competing financial interests or personal relationships that could have appeared to influence the work reported in this paper.

Acknowledgments

This work was partially supported by the FSE-REACT-EU, PON Ricerca e Innovazione 2014–2020 DM 1062/202, Cod: 19-G-12549–3. This research was funded by MIUR, grant number 2017PBXPN4, 2017FJCPEX and 2020CBEYHC (AStraLI).

References

[1] M.M. Richter, Electrochemiluminescence (ECL), Chem. Rev. 104 (2004) 3003–3036, https://doi.org/10.1021/cr020373d.
[2] D.M. Hercules, Chemiluminescence Resulting from Electrochemically Generated Species, Science 145 (1964) 808–809, https://doi.org/10.1126/science.145.3634.808.
[3] W. Miao, Electrogenerated Chemiluminescence and Its Biorelated Applications, Chem. Rev. 108 (2008) 2506–2553, https://doi.org/10.1021/cr068083a.
[4] P. Dutta, D. Han, B. Goudeau, D. Jiang, D. Fang, N. Sojic, Reactivity mapping of luminescence in space: Insights into heterogeneous electrochemiluminescence

bioassays, Biosens. Bioelectron. 165 (2020) 112372, https://doi.org/10.1016/j.bios.2020.112372.
[5] A. Zanut, A. Fiorani, S. Canola, T. Saito, N. Ziebart, S. Rapino, S. Rebeccani, A. Barbon, T. Irie, H.-P. Josel, F. Negri, M. Marcaccio, M. Windfuhr, K. Imai, G. Valenti, F. Paolucci, Insights into the mechanism of coreactant electrochemiluminescence facilitating enhanced bioanalytical performance, Nat. Commun. 11 (2020) 2668, https://doi.org/10.1038/s41467-020-16476-2.
[6] K. Sakanoue, A. Fiorani, C.I. Santo, G.Valenti Irkham, F. Paolucci, Y. Einaga, Boron-Doped Diamond Electrode Outperforms the State-of-the-Art Electrochemiluminescence from Microbeads Immunoassay, ACS Sens. 7 (2022) 1145–1155, https://doi.org/10.1021/acssensors.2c00156.
[7] Y. Feng, W. Zhou, X. Wang, J. Zhang, M. Zou, C. Zhang, H. Qi, Imaging and Simulation of Ruthenium Derivative Coating Microbeads at the Opaque Electrode with Electrogenerated Chemiluminescence, Chem. Biomed. Imaging 1 (2023) 648–658, https://doi.org/10.1021/cbmi.3c00042.
[8] H. Gao, W. Han, H. Qi, Q. Gao, C. Zhang, Electrochemiluminescence Imaging for the Morphological and Quantitative Analysis of Living Cells under External Stimulation, Anal. Chem. 92 (2020) 8278–8284, https://doi.org/10.1021/acs.analchem.0c00528.
[9] H. Ding, W. Guo, B. Su, Imaging Cell-Matrix Adhesions and Collective Migration of Living Cells by Electrochemiluminescence Microscopy, Angew. Chem. Int. Ed. 59 (2020) 449–456, https://doi.org/10.1002/anie.201911190.
[10] A. Zanut, A. Fiorani, S. Rebeccani, S. Kesarkar, G. Valenti, Electrochemiluminescence as emerging microscopy techniques, Anal. Bioanal. Chem. 411 (2019) 4375–4382, https://doi.org/10.1007/s00216-019-01761-x.
[11] S. Rebeccani, A. Zanut, C.I. Santo, G. Valenti, F. Paolucci, A Guide Inside Electrochemiluminescent Microscopy Mechanisms for Analytical Performance Improvement, Anal. Chem. 94 (2022) 336–348, https://doi.org/10.1021/acs.analchem.1c05065.
[12] Y. Liu, H. Zhang, B. Li, J. Liu, D. Jiang, B. Liu, N. Sojic, Single Biomolecule Imaging by Electrochemiluminescence, J. Am. Chem. Soc. 143 (2021) 17910–17914, https://doi.org/10.1021/jacs.1c06673.
[13] M.M. Collinson, R.M. Wightman, Observation of Individual Chemical Reactions in Solution, Science 268 (1995) (1979) 1883–1885, https://doi.org/10.1126/science.268.5219.1883.
[14] T.H. Fereja, S.A. Kitte, W. Gao, F. Yuan, D. Snizhko, L. Qi, A. Nsabimana, Z. Liu, G. Xu, Artesunate-luminol chemiluminescence system for the detection of hemin, Talanta 204 (2019) 379–385, https://doi.org/10.1016/j.talanta.2019.06.007.
[15] W. Miao, J.-P. Choi, A.J. Bard, Electrogenerated Chemiluminescence 69: The Tris (2,2'-bipyridine)ruthenium(II), (Ru(bpy)32+)/Tri-n-propylamine (TPrA) System RevisitedA New Route Involving TPrA•+ Cation Radicals, J. Am. Chem. Soc. 124 (2002) 14478–14485, https://doi.org/10.1021/ja027532v.
[16] M. Sentic, M. Milutinovic, F. Kanoufi, D. Manojlovic, S. Arbault, N. Sojic, Mapping electrogenerated chemiluminescence reactivity in space: mechanistic insight into model systems used in immunoassays, Chem. Sci. 5 (2014) 2568–2572, https://doi.org/10.1039/C4SC00312H.
[17] A. Fiorani, D. Han, D. Jiang, D. Fang, F. Paolucci, N. Sojic, G. Valenti, Spatially resolved electrochemiluminescence through a chemical lens, Chem. Sci. 11 (2020) 10496–10500, https://doi.org/10.1039/D0SC04210B.
[18] Y. Wang, B. Su, Deciphering the Mechanisms of Electrochemiluminescence by Spatially Resolved Measurements, Anal. Sens. 1 (2021) 148–155, https://doi.org/10.1002/anse.202100037.
[19] Z. Zhang, C. Ma, Q. Xu, J.-J. Zhu, Recent progress in electrochemiluminescence microscopy analysis of single cells, Analyst 147 (2022) 2884–2894, https://doi.org/10.1039/D2AN00709F.
[20] H. Ding, P. Zhou, W. Fu, L. Ding, W. Guo, B. Su, Spatially Selective Imaging of Cell–Matrix and Cell–Cell Junctions by Electrochemiluminescence, Angew. Chem. Int. Ed. 60 (2021) 11769–11773, https://doi.org/10.1002/anie.202101467.
[21] C. Ma, S. Wu, Y. Zhou, H.-F. Wei, J. Zhang, Z. Chen, J.-J. Zhu, Y. Lin, W. Zhu, Bio-Coreactant-Enhanced Electrochemiluminescence Microscopy of Intracellular Structure and Transport, Angew. Chem. Int. Ed. 60 (2021) 4907–4914, https://doi.org/10.1002/anie.202012171.
[22] C. Ma, M.-X. Wang, H.-F. Wei, S. Wu, J.-R. Zhang, J.-J. Zhu, Z. Chen, Catalytic route electrochemiluminescence microscopy of cell membranes with nitrogen-doped carbon dots as nano-coreactants, Chem. Commun. 57 (2021) 2168–2171, https://doi.org/10.1039/D0CC08223F.
[23] C. Ma, Z. Xing, X. Gou, L.-P. Jiang, J.-J. Zhu, A temperature-tuned electrochemiluminescence layer for reversibly imaging cell topography, Chem. Sci. 13 (2022) 13938–13947, https://doi.org/10.1039/D2SC04944A.
[24] D. Han, D. Fang, G. Valenti, F. Paolucci, F. Kanoufi, D. Jiang, N. Sojic, Dynamic Mapping of Electrochemiluminescence Reactivity in Space: Application to Bead-Based Assays, Anal. Chem. 95 (2023) 15700–15706, https://doi.org/10.1021/acs.analchem.3c02960.
[25] J. Dong, Y. Lu, Y. Xu, F. Chen, J. Yang, Y. Chen, J. Feng, Direct imaging of single-molecule electrochemical reactions in solution, Nature 596 (2021) 244–249, https://doi.org/10.1038/s41586-021-03715-9.
[26] M.-M. Chen, C.-H. Xu, W. Zhao, H.-Y. Chen, J.-J. Xu, Super-Resolution Electrogenerated Chemiluminescence Microscopy for Single-Nanocatalyst Imaging, J. Am. Chem. Soc. 143 (2021) 18511–18518, https://doi.org/10.1021/jacs.1c07827.
[27] J. Rodríguez-López, M. Shen, A.B. Nepomnyashchii, A.J. Bard, Scanning Electrochemical Microscopy Study of Ion Annihilation Electrogenerated Chemiluminescence of Rubrene and [Ru(bpy)3]2+, J. Am. Chem. Soc. 134 (2012) 9240–9250, https://doi.org/10.1021/ja301016n.
[28] P. Zhou, B. Su, Enhanced electrochemiluminescence at silica nanochannel membrane studied by scanning electrochemical microscopy, J. Electroanal. Chem. 904 (2022) 115943, https://doi.org/10.1016/j.jelechem.2021.115943.
[29] N. Harvey, Luminescence during Electrolysis, J. Phys. Chem. 33 (1929) 1456–1459, https://doi.org/10.1021/j150304a002.
[30] G. Merényi, J. Lind, T.E. Eriksen, Luminol chemiluminescence: Chemistry, excitation, emitter, J. Biolumin. Chemilumin. 5 (1990) 53–56, https://doi.org/10.1002/bio.1170050111.
[31] A.W. Knight, A review of recent trends in analytical applications of electrogenerated chemiluminescence, TrAC Trends Anal. Chem. 18 (1999) 47–62, https://doi.org/10.1016/S0165-9936(98)00086-7.
[32] S. Hu, Z. Cao, L. Zhou, R. Ma, B. Su, Electrochemiluminescence imaging of latent fingerprints by electropolymerized luminol, J. Electroanal. Chem. 870 (2020) 114238, https://doi.org/10.1016/j.jelechem.2020.114238.
[33] X. Jiang, Z. Wang, H. Wang, Y. Zhuo, R. Yuan, Y. Chai, A novel metal–organic framework loaded with abundant N-(aminobutyl)-N-(ethylisoluminol) as a high-efficiency electrochemiluminescence indicator for sensitive detection of mucin1 on cancer cells, Chem. Commun. 53 (2017) 9705–9708, https://doi.org/10.1039/C7CC05495E.
[34] F.-F. Wu, Y. Zhou, H. Zhang, R. Yuan, Y.-Q. Chai, Electrochemiluminescence Peptide-Based Biosensor with Hetero-Nanostructures as Coreaction Accelerator for the Ultrasensitive Determination of Tryptase, Anal. Chem. 90 (2018) 2263–2270, https://doi.org/10.1021/acs.analchem.7b04631.
[35] H. Zhang, L. Du, Z. Wei, X. Wang, N. Sojic, X. Zhou, Z. Wang, Boosting the electrochemiluminescence of luminol-O2 system by high-intensity focused ultrasound, Anal. Bioanal. Chem. 414 (2022) 8309–8315, https://doi.org/10.1007/s00216-022-04365-0.
[36] K. Wu, Y. Zheng, R. Chen, Z. Zhou, S. Liu, Y. Shen, Y. Zhang, Advances in electrochemiluminescence luminophores based on small organic molecules for biosensing, Biosens. Bioelectron. 223 (2023) 115031, https://doi.org/10.1016/j.bios.2022.115031.
[37] K.N. Swanick, S. Ladouceur, E. Zysman-Colman, Z. Ding, Self-Enhanced Electrochemiluminescence of an Iridium(III) Complex: Mechanistic Insight, Angew. Chem. Int. Ed. 51 (2012) 11079–11082, https://doi.org/10.1002/anie.201206074.
[38] W. Guo, H. Ding, C. Gu, Y. Liu, X. Jiang, B. Su, Y. Shao, Potential-Resolved Multicolor Electrochemiluminescence for Multiplex Immunoassay in a Single Sample, J. Am. Chem. Soc. 140 (2018) 15904–15915, https://doi.org/10.1021/jacs.8b09422.
[39] C. Meng, S. Knežević, F. Du, Y. Guan, F. Kanoufi, N. Sojic, G. Xu, Recent advances in electrochemiluminescence imaging analysis, EScience 2 (2022) 591–605, https://doi.org/10.1016/j.esci.2022.10.004.
[40] E. Kerr, S. Knezevic, P.S. Francis, C.F. Hogan, G. Valenti, F. Paolucci, F. Kanoufi, N. Sojic, Electrochemiluminescence Amplification in Bead-Based Assays Induced by a Freely Diffusing Iridium(III) Complex, ACS Sens. 8 (2023) 933–939, https://doi.org/10.1021/acssensors.2c02697.
[41] Y. Wang, J. Ding, P. Zhou, J. Liu, Z. Qiao, K. Yu, J. Jiang, B. Su, Electrochemiluminescence Distance and Reactivity of Coreactants Determine the Sensitivity of Bead-Based Immunoassays, Angew. Chem. Int. Ed. 62 (2023) e202216525, https://doi.org/10.1002/anie.202216525.
[42] N. Wang, H. Gao, Y. Li, G. Li, W. Chen, Z. Jin, J. Lei, Q. Wei, H. Ju, Dual Intramolecular Electron Transfer for In Situ Coreactant-Embedded Electrochemiluminescence Microimaging of Membrane Protein, Angew. Chem. Int. Ed. 60 (2021) 197–201, https://doi.org/10.1002/anie.202011176.
[43] D. Han, B. Goudeau, V. Lapeyre, V. Ravaine, D. Jiang, D. Fang, N. Sojic, Enhanced electrochemiluminescence at microgel-functionalized beads, Biosens. Bioelectron 216 (2022), https://doi.org/10.1016/j.bios.2022.114640.
[44] Z. Ding, B.M. Quinn, S.K. Haram, L.E. Pell, B.A. Korgel, A.J. Bard, Electrochemistry and Electrogenerated Chemiluminescence from Silicon Nanocrystal Quantum Dots, Science 296 (2002) (1979) 1293–1297, https://doi.org/10.1126/science.1069336.
[45] S. Zanarini, E. Rampazzo, L.Della Ciana, M. Marcaccio, E. Marzocchi, M. Montalti, F. Paolucci, L. Prodi, Ru(bpy)3 Covalently Doped Silica Nanoparticles as Multicenter Tunable Structures for Electrochemiluminescence Amplification, J. Am. Chem. Soc. 131 (2009) 2260–2267, https://doi.org/10.1021/ja8077158.
[46] G. Valenti, E. Rampazzo, S. Bonacchi, L. Petrizza, M. Marcaccio, M. Montalti, L. Prodi, F. Paolucci, Variable Doping Induces Mechanism Swapping in Electrogenerated Chemiluminescence of Ru(bpy)32+ Core–Shell Silica Nanoparticles, J. Am. Chem. Soc. 138 (2016) 15935–15942, https://doi.org/10.1021/jacs.6b08239.
[47] A. Zanut, F. Palomba, M.Rossi Scota, S. Rebeccani, M. Marcaccio, D. Genovese, E. Rampazzo, G. Valenti, F. Paolucci, L. Prodi, Dye-Doped Silica Nanoparticles for Enhanced ECL-Based Immunoassay Analytical Performance, Angew. Chem. Int. Ed. 59 (2020) 21858–21863, https://doi.org/10.1002/anie.202009544.
[48] B. Li, X. Huang, Y. Lu, Z. Fan, B. Li, D. Jiang, N. Sojic, B. Liu, High Electrochemiluminescence from Ru(bpy)32+ Embedded Metal–Organic Frameworks to Visualize Single Molecule Movement at the Cellular Membrane, Adv. Sci. 9 (2022) 2204715, https://doi.org/10.1002/advs.202204715.
[49] S. Rebeccani, C. Wetzl, V.A. Zamolo, A. Criado, G. Valenti, F. Paolucci, M. Prato, Electrochemiluminescent immunoassay enhancement driven by carbon nanotubes, Chem. Commun. 57 (2021) 9672–9675, https://doi.org/10.1039/D1CC03457J.
[50] E. Yang, H. Yang, Z. Ning, Y. Fang, M. Chen, Y. Zheng, W. Xu, G. Wu, Y. Zhang, Y. Shen, Construction of Carbon Dots with Wavelength-Tunable Electrochemiluminescence and Enhanced Efficiency, Anal. Chem. 94 (2022) 16510–16518, https://doi.org/10.1021/acs.analchem.2c04387.
[51] L. Wang, Z.-G. Wang, D. Ning, Y. Hu, S.-L. Liu, D.-W. Pang, Real-time monitoring of biomolecular dynamics on cell membranes by quantum dot-based multicolor

electrochemiluminescence, Nano. Today 50 (2023) 101855, https://doi.org/10.1016/j.nantod.2023.101855.
[52] S. Voci, B. Goudeau, G. Valenti, A. Lesch, M. Jović, S. Rapino, F. Paolucci, S. Arbault, N. Sojic, Surface-Confined Electrochemiluminescence Microscopy of Cell Membranes, J. Am. Chem. Soc. 140 (2018) 14753–14760, https://doi.org/10.1021/jacs.8b08080.
[53] S. Knežević, E. Kerr, B. Goudeau, G. Valenti, F. Paolucci, P.S. Francis, F. Kanoufi, N. Sojic, Bimodal Electrochemiluminescence Microscopy of Single Cells, Anal. Chem. 95 (2023) 7372–7378, https://doi.org/10.1021/acs.analchem.3c00869.
[54] Y. Ma, C. Colin, J. Descamps, S. Arbault, N. Sojic, Shadow Electrochemiluminescence Microscopy of Single Mitochondria, Angew. Chem. Int. Ed. 60 (2021) 18742–18749, https://doi.org/10.1002/anie.202105867.
[55] J. Descamps, C. Colin, G. Tessier, S. Arbault, N. Sojic, Ultrasensitive Imaging of Cells and Sub-Cellular Entities by Electrochemiluminescence, Angew. Chem. Int. Ed. 62 (2023) e202218574, https://doi.org/10.1002/anie.202218574.
[56] Y. Zhou, J. Dong, P. Zhao, J. Zhang, M. Zheng, J. Feng, Imaging of Single Bacteria with Electrochemiluminescence Microscopy, J. Am. Chem. Soc. 145 (2023) 8947–8953, https://doi.org/10.1021/jacs.2c13369.
[57] Y. Liu, W. Guo, B. Su, Recent advances in electrochemiluminescence imaging analysis based on nanomaterials and micro-/nanostructures, Chin. Chem. Lett. 30 (2019) 1593–1599, https://doi.org/10.1016/j.cclet.2019.05.038.
[58] W. Zhan, J. Alvarez, L. Sun, R.M. Crooks, A Multichannel Microfluidic Sensor That Detects Anodic Redox Reactions Indirectly Using Anodic Electrogenerated Chemiluminescence, Anal. Chem. 75 (2003) 1233–1238, https://doi.org/10.1021/ac026294j.
[59] F. Mavré, R.K. Anand, D.R. Laws, K.-F. Chow, B.-Y. Chang, J.A. Crooks, R. M. Crooks, Bipolar Electrodes: A Useful Tool for Concentration, Separation, and Detection of Analytes in Microelectrochemical Systems, Anal. Chem. 82 (2010) 8766–8774, https://doi.org/10.1021/ac101262v.
[60] L. Bouffier, D. Manojlovic, A. Kuhn, N. Sojic, Advances in bipolar electrochemiluminescence for the detection of biorelevant molecular targets, Curr. Opin. Electrochem. 16 (2019) 28–34, https://doi.org/10.1016/j.coelec.2019.04.004.
[61] S. Voci, A. Ismail, P. Pham, J. Yu, A. Maziz, F. Mesnilgrente, L. Reynaud, T. Livache, P. Mailley, A. Buhot, T. Leichle, A. Kuhn, L. Leroy, A. Bouchet-Spinelli, N. Sojic, Wireless Enhanced Electrochemiluminescence at a Bipolar Microelectrode in a Solid-State Micropore, J. Electrochem. Soc. 167 (2020) 137509, https://doi.org/10.1149/1945-7111/abbbc1.
[62] T.J. Anderson, P.A. Defnet, B. Zhang, Electrochemiluminescence (ECL)-Based Electrochemical Imaging Using a Massive Array of Bipolar Ultramicroelectrodes, Anal. Chem. 92 (2020) 6748–6755, https://doi.org/10.1021/acs.analchem.0c00921.
[63] T. Iwama, K.Y. Inoue, H. Abe, T. Matsue, H. Shiku, Bioimaging using bipolar electrochemical microscopy with improved spatial resolution, Analyst 145 (2020) 6895–6900, https://doi.org/10.1039/D0AN00912A.
[64] E. Villani, S. Inagi, Mapping the Distribution of Potential Gradient in Bipolar Electrochemical Systems through Luminol Electrochemiluminescence Imaging, Anal. Chem. 93 (2021) 8152–8160, https://doi.org/10.1021/acs.analchem.0c05397.
[65] S.F. Douman, D. Collins, L.R. Cumba, S. Beirne, G.G. Wallace, Z. Yue, E.I. Iwuoha, F. Melinato, Y. Pellegrin, R.J. Forster, Wireless electrochemiluminescence at functionalised gold microparticles using 3D titanium electrode arrays, Chem. Commun. 57 (2021) 4642–4645, https://doi.org/10.1039/D1CC01010G.